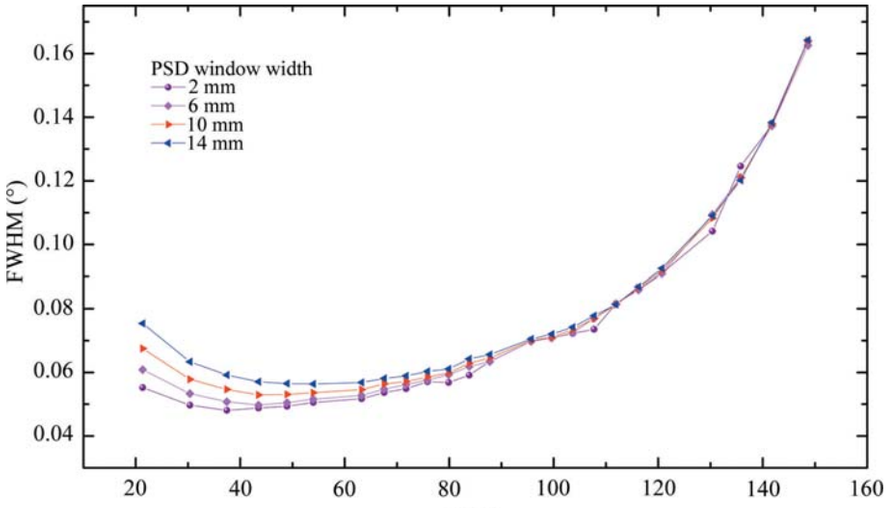

Figure 3.1.37
FWHM data from SRM 660b collected using the NIST machine configured with a Johansson IBM and PSD, illustrating the contribution to defocusing at low angles with increasing window width.

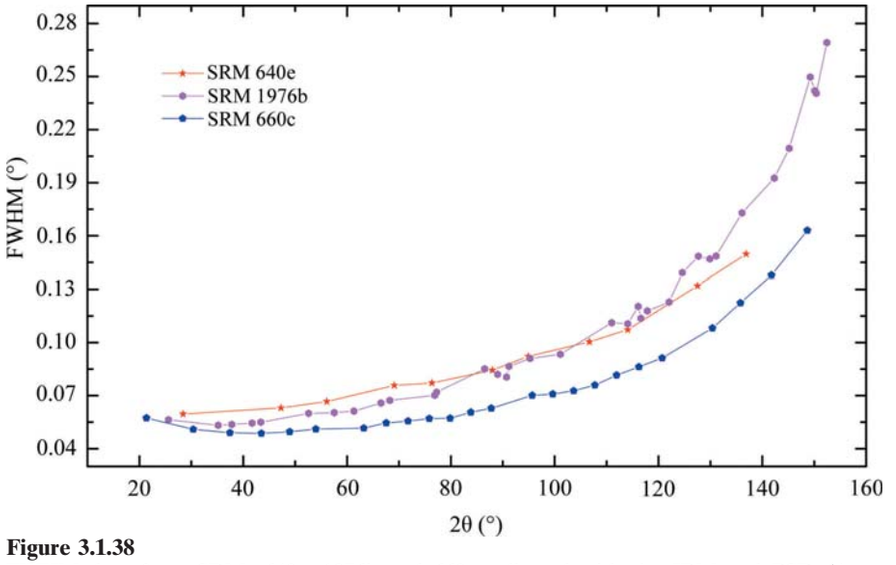

Figure 3.1.38
FWHM data from SRMs 640e, 1976b and 660c collected with the IBM and PSD (4 mm window) and fitted using the split Pearson VII PSF with uniform weighting.

ment in resolution with the reduction in the width of the PSD window is apparent, and is in accordance with expectations as per Fig. 3.1.7 of Section 3.1.2. Also, because of the $1/\tan\theta$ dependence of this broadening effect, the impact of the window size nearly vanishes above 100° 2θ.

Fig. 3.1.38 shows FWHM data obtained for SRMs 640e, 1976b and 660c using the split Pearson VII PSF, fitted using uniform weighting on data collected with the IBM and PSD with a 4 mm window. The 660c data set, which exhibits the lowest FWHM values, will be discussed first. The FPA analysis performed in the certifications of SRM 660b and 660c included a Lorentzian FWHM with a $1/\cos\theta$ dependence to account for size-induced broadening; a domain size of approximately 0.7 to 0.8 μm was indicated. There is a high level of uncertainty in these values, as they are reflective of an exceedingly small degree of broadening, the detection of which is near the resolution limit of the equipment. The term varying as $\tan\theta$, interpreted as microstrain, refined to zero. These values are found in the CoA for the SRMs. The linear attenuation coefficient for a compact of LaB_6, with an intrinsic linear attenuation of 1125 cm^{-1} and a particle-packing factor of 60 to 70%, would be approximately 800 cm^{-1}. Therefore, the contribution to the observed FWHM from specimen transparency with SRM 660c is negligible, as illustrated in Fig. 3.1.10. Likewise, the FPA analysis performed for the certification of SRM 640e included size and microstrain terms; a smaller crystallite size of 0.6 μm was obtained with a very slight amount of microstrain broadening. However, the linear attenuation coefficient for silicon is 148 cm^{-1}; for a powder compact it would be approximately 100 cm^{-1}. The transparency of this specimen would lead to significant broadening. (See Fig. 3.1.10 for the effect of an attenuation of 100 cm^{-1}.) Therefore, these three effects, in combination, would be expected to lead to a small degree of broadening throughout the 2θ range for SRM 640e, but with a substantial effect in the mid-angle region because of the $\sin 2\theta$ dependence of the transparency aberration. Lastly, SRM 1976b is a sintered compact of near theoretical density; therefore, considering the linear attenuation coefficient for alumina, 126 cm^{-1}, a value for the actual SRM 1976b specimen of somewhat less than this is expected. An FPA analysis of SRM 1976b indicates a domain size of 1 μm, but with a significant degree of Gaussian microstrain broadening; this is evident in the observed increase in FWHM with 2θ angle shown in Fig. 3.1.38. We conclude that the FWHM data from all three SRMs shown in Fig. 3.1.38 are in correspondence with expectations and can be used to select which SRM is best suited for a given application. We do not, however, recommend using an SRM other than SRM 660*x* for a microstructure analysis. It should be added that fitting the profiles of SRM 1976b is complicated by the fact that many of them overlap; this leads to the oscillations in the FWHM values shown in Fig. 3.1.38 for this SRM. The origins of this difficulty were discussed in Section 3.1.5 and can be addressed with the use of the Caglioti function.

With the use of model-based methods for calibration and subsequent data analysis, it is appropriate to consider a strategy for the refinement of the available parameters. The successful refinement will yield the right answer and, with the use of models that make sound physical sense with respect to the experimental design, a good fit to the observation. The refinement strategies for both FPA and Rietveld analyses can be based on a consideration of which terms are specific to the IPF and the manner in which they can be determined. Several parameters can be measured explicitly from experiments other than the diffraction experiment under examination. Examples of these 'well determined' parameters include the goniometer zero angles and the incident- and receiving-slit sizes. Conversely, indeterminate metrics that can only be determined through the diffraction experiment itself include the impact of the post-monochromator on the Cu $K\alpha_1/K\alpha_2$ ratio and the degree of axial divergence. Indeterminate parameters specific to the IPF are only refined using high-quality data from standards and are fixed for subse-